

Controlling the spin of Co atoms on Pt(111) by hydrogen adsorption

Q. Dubout,¹ F. Donati,¹ C. Wäckerlin,¹ F. Calleja,^{1,2} M. Etzkorn,^{1,3}
A. Lehnert,¹ L. Claude,¹ P. Gambardella,^{1,4} and H. Brune¹

¹*Institute of Condensed Matter Physics (ICMP),*

École Polytechnique Fédérale de Lausanne (EPFL), Station 3, CH-1015, Switzerland

²*Madrid Institute for Advanced Studies, IMDEA Nanoscience,
Calle Faraday 9, Campus Cantoblanco, E-28049 Madrid, Spain*

³*Max Planck Institute for Solid State Research, Heisenbergstr. 1, 70569 Stuttgart, Germany*

⁴*Department of Materials, ETH Zürich, Hönggerberggring 64, CH-8093 Zürich, Switzerland*

REVERSIBLE HYDROGEN ADSORPTION

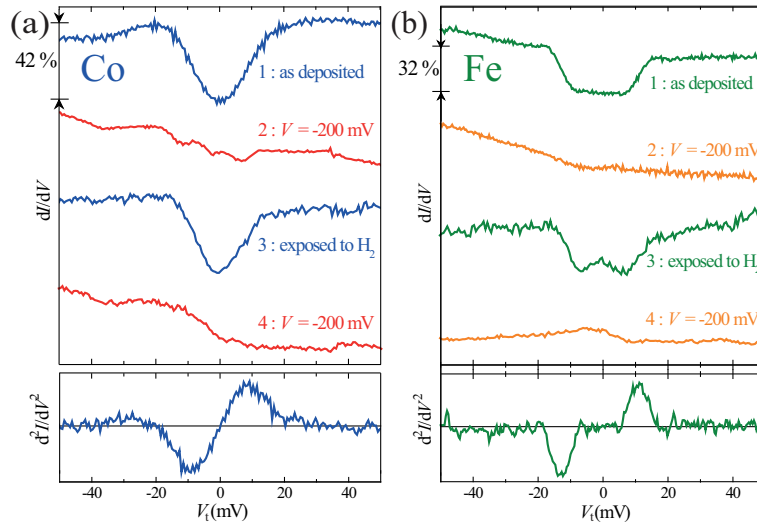


FIG. S1. Sequence of dI/dV spectra acquired alternately on hydrogenated and clean Co (a), and Fe (b) adatom on Pt(111), as found directly after deposition (1), after a voltage pulse at -200 mV (2), after exposure to H_2 (3), and after a final -200 mV pulse (4) ($V_t = -50$ mV, $I_t = 1$ nA, $V_{mod} = 2.8$ mV, $T = 4.4$ K). Both Co and Fe hydrogenated adatoms display inelastic features, evidenced as peaks in d^2I/dV^2 . The curve displayed is the numerical derivative of (1). Note that these experimental conditions (temperature and lock-in modulation) do not allow to detect the low energy spin-excitation found for Fe atoms on Pt(111) in Ref. [43].

THRESHOLD VOLTAGE FOR HYDROGEN DESORPTION

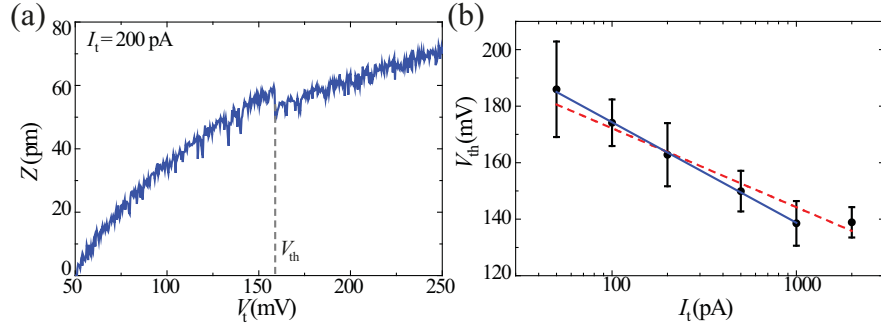


FIG. S2. (a) Vertical displacement $z(V)$ curve acquired on top of a CoH complex. Hydrogen desorption is seen as a sharp downward step, as indicated by the grey dashed line ($I_t = 200$ pA, $T = 4.4$ K). (b) Hydrogen desorption voltage versus tunnel current. Each data point corresponds to the average V_{th} at which a jump in z was observed while ramping the voltage at constant current. Average over 10 CoH complexes. The solid blue line is a linear fit to the first five points and the dashed red line is a fit to the six points. The threshold V_{th} decreases exponentially with I_t , until it reaches a minimum value of about 140 mV.

COBALT TRIHYDRIDE

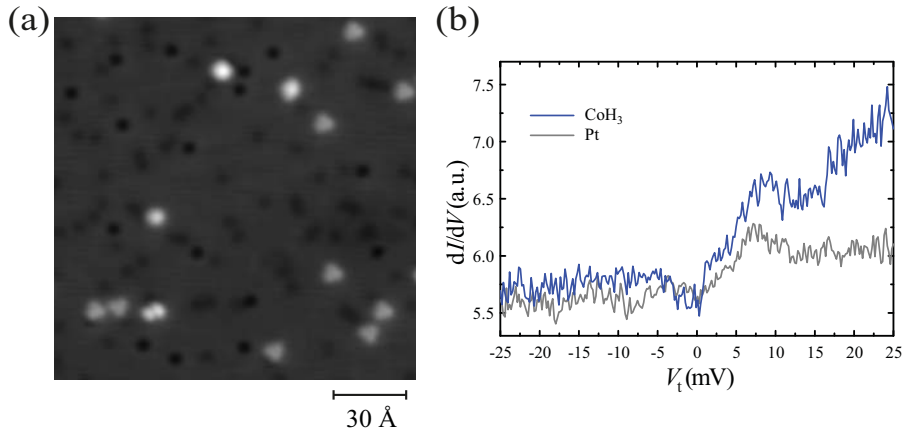


FIG. S3. (a) STM image of a Co/Pt(111) sample that has been exposed to more H_2 . Most of the CoH_n complexes appear as triangles with two possible orientations ($V_t = -50$ mV, $I_t = 83$ pA, $T = 4.4$ K). (b) dI/dV spectrum of a triangular CoH_3 complex. A spectrum acquired directly over the Pt(111) surface is also shown for comparison ($V_t = -25$ mV, $I_t = 0.5$ nA, $V_{mod} = 1$ mV, $T = 4.4$ K).

ABSENCE OF FIELD DEPENDENCE FOR HIGHER ENERGY EXCITATIONS

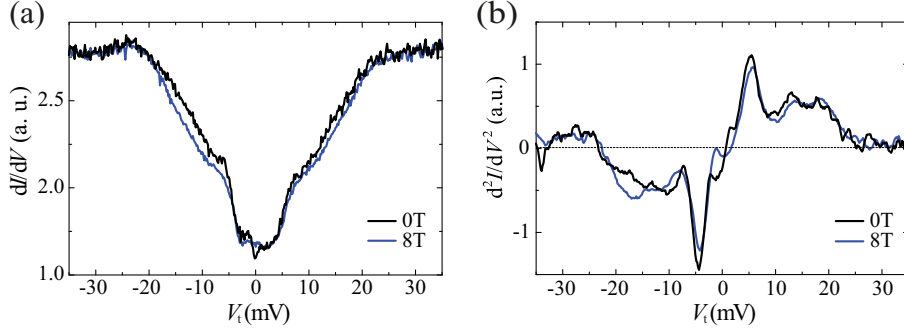


FIG. S4. (a) dI/dV spectra of two similar fcc-adsorbed CoH complexes at 0 and 8 T applied perpendicularly to the sample ($V_t = -45$ mV, $I_t = 0.75$ nA, $V_{mod} = 1$ mV, $T = 0.4$ K). (b) numerical derivative of (a).

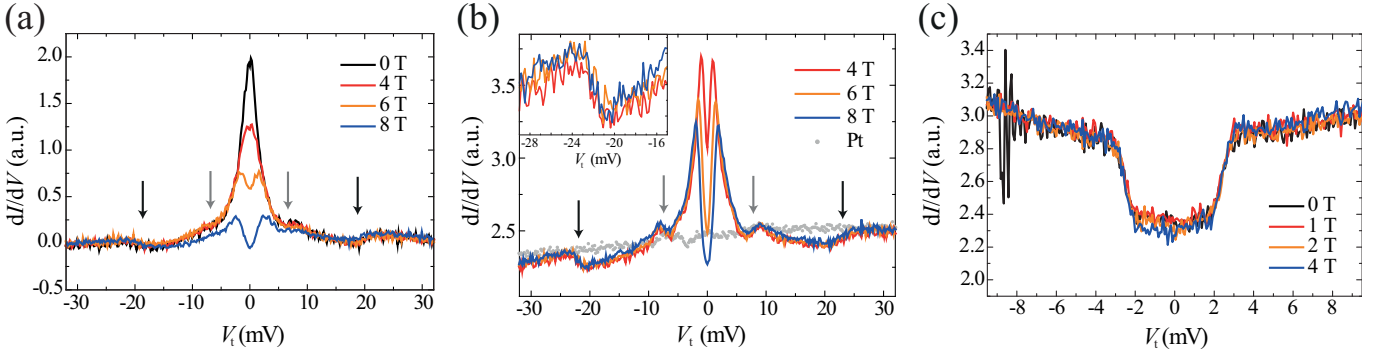


FIG. S5. (a) dI/dV spectra obtained over a fcc-adsorbed CoD_2 complex while applying an out-of-plane magnetic field ranging between 0 and 8 T. A parabolic background was subtracted from each spectrum ($V_t = -50$ mV, $I_t = 0.75$ nA, $V_{mod} = 1$ mV peak-to-peak, $T = 4.4$ K). (b) A similar series of spectra acquired on a CoHD complex at $T = 0.4$ K. A spectrum obtained on clean Pt(111) is shown for reference. Inset: magnification of an inelastic step emphasizing its insensitivity to external magnetic fields. In (a) and (b), the black and gray arrows mark the inelastic vibrational features whose energy thresholds allow distinguishing the CoHD and CoD_2 complexes from the CoH_2 one. None of these modes display field-dependence. (c) dI/dV spectra obtained over a hcp-adsorbed CoH_2 complex while applying an out-of-plane magnetic field ranging from 0 to 4 T ($V_t = -10$ mV, $I_t = 0.25$ nA, $V_{mod} = 500$ μV , $T = 0.4$ K).

EIGENSTATES OF THE SPIN HAMILTONIAN FOR FCC-ADSORBED COH

TABLE I. Projection onto a m -states basis of the first two eigenstates of fcc-adsorbed CoH complexes obtained diagonalizing Eq. 1 of the main text with $S = 2$, $g = 2.1$, $D = -3$ meV, and $E = 0.6$ meV.

$B = 0$ T	$m = +2$	$m = +1$	$m = 0$	$m = -1$	$m = -2$
Ψ_0	0.697	0	-0.166	0	0.697
Ψ_1	0.707	0	0	0	-0.707
$B = 4$ T	$m = +2$	$m = +1$	$m = 0$	$m = -1$	$m = -2$
Ψ_0	0.083	0	-0.120	0	0.989
Ψ_1	0.988	0	-0.117	0	-0.097

KONDO LINESHAPE IN ABSENCE OF A MAGNETIC FIELD

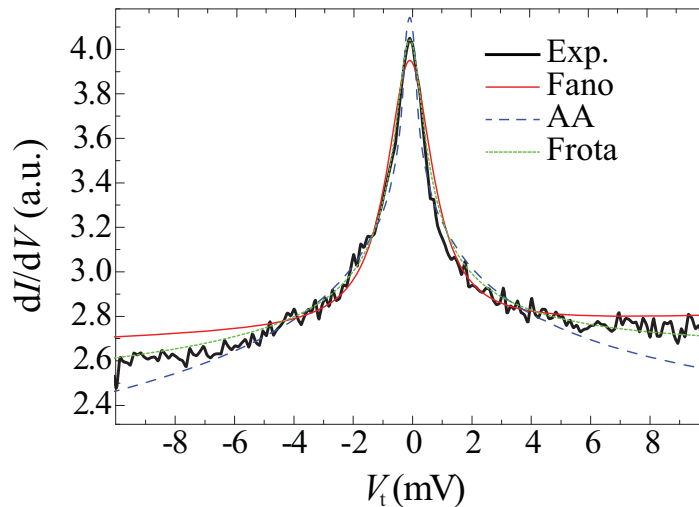


FIG. S6. dI/dV spectrum obtained over a fcc-adsorbed CoH_2 complex at 0 T and 0.4 K. $V = -15$ mV, $I_t = 0.1$ nA, $V_{mod} = 500 \mu\text{V}$. Fits are based on the Frota, Fano and Anderson-Appelbaum models (Eqs. (S1), (S3), (S2)). A linear background is added to the fits.

In Fig. S6, least-square fits based on the Fano, Frota and Anderson-Appelbaum (AA) models [31–35] are compared. Equation (S1) gives the expression for the many-body density of states (DOS) of a Fano resonance [31]:

$$g_{Fano}(E) = \frac{(E/\Gamma_{Fano} + q)^2}{(E/\Gamma_{Fano})^2 + 1}, \quad (\text{S1})$$

with the linewidth Γ_{Fano} , and the Fano parameter q . In the Anderson-Appelbaum (AA) model [33–35], the many-body DOS is given by:

$$g_{AA}(E) = \left[\int_{-\omega_0}^{\omega_0} \frac{f(E')}{E - E'} dE' * \frac{df(E)}{dE} \right], \quad (\text{S2})$$

with $f(E) = (1 + \exp[E/(k_B T)])^{-1}$ being the Fermi-Dirac distribution, $[a(x) * b(x)]$ the convolution between $a(x)$ and $b(x)$, and ω_0 the cutoff energy for the integration. Using $\omega_0 = 100$ meV, we evaluated $g_{AA}(E)$ numerically for different temperatures T including a correction $-\ln(1 + E/\omega_0)$ which compensates for ω_0 not being infinitely large [33] and stored the precomputed results for later use in the numerical fits.

The many-body DOS for the Frota model [32] is given in Eq. (S3)

$$g_{Frota}(E) = -\text{Re}(\sqrt{i\tilde{\Gamma}/(i\tilde{\Gamma} + E)}), \quad (\text{S3})$$

with Re being the real part and $\tilde{\Gamma}$ the peak linewidth. Simulated dI/dV spectra are then obtained convoluting the corresponding many-body DOS with the lock-in voltage modulation V_{mod} :

$$dI/dV(eV) \propto \left[g(E = eV) * e\sqrt{(V_{mod}^2 - V^2)} \right], \quad (\text{S4})$$

where the function $g(E = eV)$ may be chosen to be $g_{AA}(E)$, $g_{Fano}(E)$ or $g_{Frota}(E)$. The Fano-lineshape fails to reproduce the tails of Kondo-resonance. The AA-model partially reproduces the tails of the Kondo resonance but yields a too narrow lineshape at the Kondo-peak. The Frota model best reproduces the Kondo lineshape, see Fig. S6.

In order to extract the Frota intrinsic linewidth Γ as a function of the temperature, we subtract the contribution of the tip thermal broadening in a quadratic approximation $\Gamma = \sqrt{\tilde{\Gamma}^2 - \Gamma_{tip}^2}$. Here, we assume the tip thermal broadening Γ_{tip} to be proportional to the half-width-half-maximum of the derivative of Fermi-Dirac distribution $W_{FD} = \frac{1}{2}3.5k_B T$. More precisely, $\Gamma_{tip} = W_{FD}/2.54$, where the factor 1/2.54 is due to the ratio between the Frota intrinsic width and the corresponding half-width-half-maximum [35, 38].

KONDO LINESHAPE IN APPLIED MAGNETIC FIELD

The expression for the conductance in applied magnetic field $\sigma(E)$ is [26–28, 33–35]:

$$\begin{aligned} \sigma(E) &= \sigma_1(E) + \sigma_2(E), \\ \sigma_1(E) &= c_1 \left[\frac{1}{3} + \frac{2}{3} \sum_{i,f;i \neq f} \rho_i(T) \left[\Theta\left(\frac{\Delta_{if} + E}{k_B T}\right) + \Theta\left(\frac{\Delta_{if} - E}{k_B T}\right) \right] \right], \\ \sigma_2(E) &= c_2 \sum_{i,f;i \neq f} \rho_i(T) \left(\left[\Theta\left(\frac{\Delta_{if} + E}{k_B T}\right) + \Theta\left(\frac{\Delta_{if} - E}{k_B T}\right) \right] g(E) \right. \\ &\quad \left. + \left[\Theta\left(\frac{\Delta_{if} + E}{k_B T}\right) + \frac{1}{2} \right] g(E + \Delta_{if}) \right. \\ &\quad \left. + \left[\Theta\left(\frac{\Delta_{if} - E}{k_B T}\right) + \frac{1}{2} \right] g(E - \Delta_{if}) \right). \end{aligned} \quad (\text{S5})$$

Here, $\rho_i(T) = (\exp[-E_i/(k_B T)]) / (\sum_i \exp[-E_i/(k_B T)])$ is the thermal occupation of the spin in state i , $\Theta(x) = [1 + (x - 1) \exp(x)] [1 - \exp(x)]^{-2}$ is the thermally broadened step-function, and Δ_{if} is the energy separation of the spin states i, f . The ratio of the prefactors c_1/c_2 sets the relative amplitudes of the spin excitation (σ_1) and the Kondo (σ_2) contributions to the conductance. Again, the function $g(E)$ may be chosen to be $g_{AA}(E)$, $g_{Fano}(E)$ or $g_{Frota}(E)$. Fits in Fig. 3(d) of the manuscript are obtained using $g(E) = g_{Frota}(E)$. Finally, simulated dI/dV spectra are then obtained convoluting the conductance σ with the lock-in voltage modulation:

$$dI/dV(eV) \propto \left[\sigma(E = eV) * e\sqrt{(V_{mod}^2 - V^2)} \right]. \quad (\text{S6})$$